haematologica
Journal of the Ferrata Storti Foundation

Mutual amplification of sensory nerve outgrowth and tumor progression in myeloma

by Motosumi Nakagawa, Masahiro Hiasa, Jumpei Teramachi, Takeshi Harada, Asuka Oda, Go Nishino, SooHa Matsuki, Mariko Hanawa, Ariunzaya Bat-Erdene, Takako Taniguchi, Hisaaki Taniguchi, Koichi Tsuneyama, Tatsuya Tominaga, Eiji Tanaka, Takeshi Y. Hiyama, Ken-ichi Matsuoka, Yoshio Katayama and Masahiro Abe

Received: November 27, 2025.
Accepted: February 18, 2026.

Citation: Motosumi Nakagawa, Masahiro Hiasa, Jumpei Teramachi, Takeshi Harada, Asuka Oda, Go Nishino, SooHa Matsuki, Mariko Hanawa, Ariunzaya Bat-Erdene, Takako Taniguchi, Hisaaki Taniguchi, Koichi Tsuneyama, Tatsuya Tominaga, Eiji Tanaka, Takeshi Y. Hiyama, Ken-ichi Matsuoka, Yoshio Katayama and Masahiro Abe. Mutual amplification of sensory nerve outgrowth and tumor progression in myeloma. Haematologica. 2026 Feb 26. doi: 10.3324/haematol.2025.300309 [Epub ahead of print]

Mutual amplification of sensory nerve outgrowth and tumor progression in myeloma

Authors

Motosumi Nakagawa[1], Masahiro Hiasa[1], Jumpei Teramachi[2], Takeshi Harada[3], Asuka Oda[3], Go Nishino[1], SooHa Matsuki[1], Mariko Hanawa[1], Ariunzaya Bat-Erdene[4], Takako Taniguchi[5], Hisaaki Taniguchi[5], Koichi Tsuneyama[6], Tatsuya Tominaga[7], Eiji Tanaka[1], Takeshi Y Hiyama[8], Ken-ichi Matsuoka[3], Yoshio Katayama[9] and Masahiro Abe[10]

1. Department of Orthodontics and Dentofacial Orthopedics, Tokushima University Graduate School of Biomedical Sciences, Tokushima, Japan.
2. Department of Oral Function and Anatomy, Graduate School of Medicine, Dentistry and Pharmaceutical Sciences, Okayama University Graduate School, Okayama, Japan.
3. Department of Hematology, Endocrinology and Metabolism, Tokushima University Graduate School of Biomedical Sciences, Tokushima, Japan.
4. Department of Immunology, School of Bio-Medicine, Mongolian National University of Medical Sciences, Ulaanbaatar, Mongolia; Department of Health Research, Graduate School of Mongolian National University of Medical Sciences, Ulaanbaatar, Mongolia.
5. Division of Disease Proteomics, Institute for Enzyme Research, University of Tokushima, Tokushima, Japan
6. Department of Pathology and Laboratory Medicine, Tokushima University Graduate School of Biomedical Sciences, Tokushima, Japan.
7. Department of Bioanalytical Technology, Tokushima University Graduate School of Biomedical Sciences, Tokushima, Japan.
8. Department of Integrative Physiology, Tottori University Graduate School and Faculty of Medicine, Tottori University, Tottori, Japan.
9. Hematology, Kobe University Hospital, Kobe, Japan.
10. Department of Hematology, Kawashima Hospital, Tokushima, Japan.

Correspondence

Masahiro Hiasa, mhiasa@tokushima-u.ac.jp

Jumpei Teramachi, jumptera@okayama-u.ac.jp

Short Title

Sensory nerve–tumor crosstalk in myeloma

Funding

This work was supported by AMED-CREST (grant number JP21gm1510001 to T.H., T.Y.H., Y.K., and M.A.), Grants-in-Aid for Scientific Research (23K27791 and 24K22250 to M.H.; 24K02643 and 22K19626 to J.T.) from the Japan Society for the Promotion of Science, and the IMS Career Development Award (2CDA100025 to A.B.). The funders had no role in study design, data collection and analysis, decision to publish, or preparation of the manuscript.

Author Contributions

M.N., M.H., T.Y.H., Y.K., and M.A. conceived and designed the study. M.N., M.H., G.N., and M.Ha. performed animal experiments. M.N., M.H., and G.N. performed bone specimen clearing and immunostaining. M.N., M.H., J.T., S.M., T.H., A.O., A.B., and K.M. performed cell culture and Western blotting. T.H., A.O., J.T., and K.T. performed immunohistochemical analyses. T.H., A.O., M.H., and J.T. performed transfection. J.T., T.Ta., and H.T. performed secretome analyses. M.N., J.T., S.M., and T.To. performed EV analyses. M.N., M.H., J.T., T.H., T.To., H.T., T.Ta., E.T., K.M., and M.A. analyzed data. M.N., M.H., and M.A. wrote the manuscript. All authors reviewed and approved the final version of the manuscript.

Authors Disclosures

M.A. received research funding from Sanofi K.K., and honoraria from Takeda Pharmaceutical, Janssen Pharmaceutical and Daiichi Sankyo Company.

Data sharing

Reasonable requests for reagents and data should be addressed to the corresponding authors. Detailed proteomic analyses will be published elsewhere.

Multiple myeloma (MM) is characterized by preferential accumulation of tumor cells in bone marrow with devastating bone destruction. Bone pain is a common and debilitating complication associated with osteoclastic bone destruction in MM and cancer metastasis to bone. Excitation and sensitization of sensory nerves (SNs) evoke pain. Calcitonin gene-related peptide (CGRP)-positive SNs have been reported to increase and intermingle with MM cells in bone marrow in mouse MM models[1]. SNs extend their neurites in acidic conditions in MM bone marrow lesions in mouse MM models with SN excitation as shown by phosphorylation of ERK1/2 and CREB in dorsal root ganglia (DRG), suggesting an important role of acid in sprouting of SN neurites and increased susceptibility to pain[1]. Tumor innervation has been recently drawing considerable attention in growth, metastasis/invasion, and drug resistance in various cancers[2, 3]. However, little is known on SN distribution in the bone marrow and the interactions between SNs and bone-residing tumors such as MM. Precise evaluation of SN distribution in the bone marrow is difficult in thin-sliced tissue specimens and requires a three-dimensional SN visualization in the entire bone marrow. In the present study, we therefore aimed to three-dimensionally explore SN spreading and outgrowth in the bone marrow and clarify the underlying mechanisms of SN sprouting in MM and the role of SNs in MM tumor progression. We demonstrate here that sensory innervation is increased in the bone marrow with MM lesions. Interestingly, MM cells induce SN outgrowth, which in turn promotes MM tumor progression to form a vicious cycle, posing the concept of MM progression being controlled by the peripheral nervous system.

Peripheral nerves are distributed throughout the body. In order to explore the actual state of $CGRP^+$ SN distribution in the bone marrow in three dimensions, we visualized SNs in bone in MM models after transparency of the entire bone by the optical clearing CUBIC method[4, 5]. The distribution and density of $CGRP^+$ SNs increased in the bone marrow of tibiae in different MM models implanted intra-tibially with human MM.1S and RPMI8226, and mouse Vk12598 and 5TGM1 MM cell lines, compared with control contralateral tibiae without MM tumor involvement in the same mice (Figure 1A, Supplementary Figure 1A). These results suggest that sensory innervation is enhanced in the bone marrow in MM.

To dissect the mechanisms for the SN outgrowth, we first asked if MM cells produce SN outgrowth-promoting activity. MM cell culture supernatants enhanced the neurite sprouting and outgrowth of SNs derived from the neural cell line Neuro2a and primary mouse DRG cells as estimated according to the previously reported investigation system[6] (Figure 1B). We reported that TGF-β-activated kinase 1 (TAK1) plays pivotal role in tumor progression and drug resistance along with alteration of bone marrow microenvironment in MM, including bone metabolism and angiogenesis[7]. Through further exploring the role of

TAK1 in the microenvironmental alteration, we recently found that pretreatment on MM cells with the TAK1 inhibitor LLZ1640-2 abolished the SN neurite outgrowth promoting activity by MM cells (Supplementary Figure 1B). To elucidate MM cell-derived secreted factor(s) to promote SN neurite outgrowth, we therefore performed a comprehensive secretome analysis of MM cell lines in the presence or absence of LLZ1640-2 (Supplementary Figure 2). We selected TAK1-dependent MM cell-specific factors with high basal secretion levels (Supplementary Figure 2F), which included factors involved in the biology of the nervous system. We then screened their neurite outgrowth-promoting activity. Among the secreted MM cell-specific factors, neogenin1 (NEO1) was secreted at high basal levels from MM cells; and recombinant (r)NEO1 was found to potently enhance neurite sprouting and outgrowth in Neuro2a-derived SNs in the presence of NGF and DRG cells (Figure 1C and Supplementary Figure 1C). We confirmed NEO1 secretion from primary MM cells as well as MM cell lines (Supplementary Figure 1D,E). When NEO1 was depleted from MM cell culture supernatants, their neurite outgrowth-promoting activity almost disappeared (Figure 1D and Supplementary Figure 1D,E). To further clarify the role of MM cell-derived NEO1, we created *NEO1*-knockout (KO) RPMI8226 cells. The KO cells mitigated the *in vitro* neurite outgrowth of Neuro2a-derived SNs compared with control RPMI8226 cells, which was reversed by addition of rNEO1 (Figure 1E). These results suggest soluble NEO1 as a critical MM cell-derived SN neurite elongation factor.

Membrane-bound NEO1 is expressed in peripheral nerves as a receptor for neural guidance and repulsion molecules[8]. RGM-a, a repulsive guidance molecule, is one of major NEO1 ligands which is abundantly contained in sera[9, 10]. RGM-a has been demonstrated to induce neurite retraction and axonal growth cone collapse[11]. rRGM-a suppressed neurite outgrowth induction by NGF (Figure 2A); however, addition of rNEO1 inhibited the rRGM-a's action (Figure 2B and Supplementary Figure 3A). rRGM-a also acutely retracted neurites when added to Neuro2a-derived SNs with extended neurites (Figure 2C, Supplementary Figure 3B) and disappeared their actin polymerization (Figure 2D, Supplementary Figure 3C). Addition of rNEO1 almost completely inhibited the RGM-a-induced neurite retraction and actin depolymerization. Therefore, soluble NEO1 from MM cells can induce neurite outgrowth at least in part through acting as a decoy receptor to inhibit RGM-a. However, rNEO1 still enhanced the neurite extension in a serum-free condition (Supplementary Figure 3D), suggesting a mechanism besides RGM-a-mediated one. NEO1 contains six fibronectin type III domains that can interact with integrin β_1 through an Arg-Gly-Asp (RGD) amino acid sequence to induce the activation of downstream signaling pathways, including the ERK/MAP kinase pathway. Soluble NEO1 can also interact with growth factors such as bone morphogenetic proteins and extracellular matrix components. These characteristic

features endow soluble NEO1 with additional activities which membrane-bound NEO1 does not have.

Bone marrow microenvironment is skewed by MM cell infiltration, which is vital for MM cell growth and survival. SN outgrowth may also affect the bone marrow microenvironment in MM. Therefore, we next explored the effects of SNs on MM cell growth. MM cell growth was enhanced when cocultured with Neuro2a-derived SNs or DRG cells (Figure 3A). Extracellular vesicles (EVs) are recognized as crucial mediators of cellular communication in various pathological conditions including those in the nervous system and tumor microenvironment[12]. We therefore isolated EVs from culture supernatants of primary DRG cells as well as Neuro2a-derived SNs as previously described[13]. The isolated EVs also showed potent MM cell proliferation activity (Figure 3B). miR-21, an oncogenic microRNA, has been reported to contribute to perineural invasion and proliferation of cancers[14]. As assumed, pre-treatment of DRG cells with an miR-21 inhibitor abrogated MM cell growth enhancement by DRG cell-derived EVs (Figure 3C). Therefore, SN expansion in the bone marrow is suggested to promote MM cell growth at least in part through SN-secreted EVs.

To further confirm the role of SNs in MM tumor growth, we next examined the MM tumor progression in mice with or without pharmacological sensory denervation. Pharmacological denervation of SNs was performed by subcutaneous injection of high-dose capsaicin into a lumbar dorsal region according to the previously reported method[15]. Although capsaicin did not apparently affect the growth of MM cell lines *in vitro* (data not shown), we waited for 7 days after the last capsaicin injection to remove capsaicin out of the mice and degenerate SNs. SN fibers were found to be substantially decreased in the bone marrow by the pharmacological sensory denervation (Figure 3D, upper). Then, mouse 5TGM1 and human JJN3 MM cells were intra-tibially inoculated. MM tumor growth was notably reduced in the mice with the sensory denervation compared to control mice (Figure 3D), suggesting a critical role of SNs in MM tumor growth. Furthermore, SN spreading in the bone marrow was reduced in tibiae bearing *NEO1*-KO RPMI8226 cells compared with those with control RPMI8226 cells (Figure 3E). IVIS images showed that tumor growth was also attenuated with the *NEO1*-KO cells, although there was no clear difference of *in vitro* growth between the *NEO1-KO* and control cells (Supplementary Figure 3E), suggesting the critical roles of MM cell-derived NEO1 in neurite outgrowth of SNs and MM cell growth.

The present study highlights that sensory innervation is increased in the bone marrow in MM, which in turn promotes MM tumor growth to form a vicious cycle between SN hyperplasia and tumor progression in MM. Mechanistically, we found that MM cell-

derived soluble NEO1 is a critical mediator for enhancement of sensory innervation in MM. Furthermore, we demonstrated that SNs enhance MM cell growth at least in part through SN-secreted EVs. SNs extend their axons to enhance nociception in acidic conditions in MM bone marrow lesions in mouse models with up-regulation of pERK1/2 and pCREB, indicators for neuron excitation, in DRG[1]. Soluble NEO1 further enhanced neurite outgrowth induced in acidic conditions (Supplementary Figure 3F), suggesting that soluble NEO1 robustly enhances neurite outgrowth in the tumor acidic environment to facilitate the nociception to evoke pain in acidic conditions. Collectively, these results implicate SNs as a new niche component in MM, as there has been no previous concept of MM tumor progression being controlled by the peripheral nervous system. Dynamic crosstalk between cancer cells and the peripheral nervous system has been revealed in various types of cancers. MM cells may preferentially reside and colonize in the close vicinity of sensory nerves in bone marrow, which should be deciphered with sophisticated live imaging techniques.

SN distribution is not even in the bone marrow; therefore, it is hard to assess SN density and distribution in the whole bone marrow, using small bone marrow biopsy samples from patients with MM. To address clinical relevance of the present observations, the levels of SN-derived mediators such as CGRP in combination with the levels of soluble NEO1 in bone marrow plasma should be explored in parallel with development of novel electrophysiological techniques to directly probe SN activity in the bone marrow. Future research will further characterize the neuronal behavior for cell-to-cell interactions with tumor cells as well as microenvironmental cells in MM bone marrow, including vascular, bone and immune cells, besides pain sensation.

All procedures involving human samples from healthy donors and patients were performed with written informed consent in accordance with the Declaration of Helsinki and a protocol approved by the Institutional Review Board for human protection at University of Tokushima (Permission number: 2638-4). This study was also approved by the Genetic Modification Experiment Safety Management Committee of Tokushima University (Permit No. 2024-10). All animal experiments were conducted under the regulation and permission of the Animal Care and Use Committee of Tokushima University, Tokushima, Japan (Permit No. T2022-94).

References

1. Hiasa M, Okui T, Allette YM, et al. Bone Pain Induced by Multiple Myeloma Is Reduced by Targeting V-ATPase and ASIC3. Cancer Res. 2017;77(6):1283-1295.
2. Ji ZZ, Chan MK, Tang PC, et al. Tumor Innervation: From Bystander to Emerging Therapeutic Target for Cancer. Int J Mol Sci. 2025;26(18):9257.
3. Winkler F, Venkatesh HS, Amit M, et al. Cancer neuroscience: State of the field, emerging directions. Cell. 2023;186(8):1689-1707.
4. Tainaka K, Murakami TC, Susaki EA, et al. Chemical Landscape for Tissue Clearing Based on Hydrophilic Reagents. Cell Rep. 2018;24(8):2196-2210.e2199.
5. Thai J, Fuller-Jackson JP, Ivanusic JJ. Using tissue clearing and light sheet fluorescence microscopy for the three-dimensional analysis of sensory and sympathetic nerve endings that innervate bone and dental tissue of mice. J Comp Neurol. 2024;532(1):e25582.
6. Popko J, Fernandes A, Brites D, Lanier LM. Automated analysis of NeuronJ tracing data. Cytometry A. 2009;75(4):371-376.
7. Teramachi J, Tenshin H, Hiasa M, et al. TAK1 is a pivotal therapeutic target for tumor progression and bone destruction in myeloma. Haematologica. 2021;106(5):1401-1413.
8. Wilson NH, Key B. Neogenin: one receptor, many functions. Int J Biochem Cell Biol. 2007;39(5):874-878.
9. Shimizu M, Shiraishi N, Tada S, et al. RGMa collapses the neuronal actin barrier against disease-implicated protein and exacerbates ALS. Sci Adv. 2023;9(47):eadg3193.
10. Schreier P, Huang L, Fung E, et al. Development and validation of an ultra-performance liquid chromatography with tandem mass spectrometry method for determination of soluble repulsive guidance molecule A in human serum and cerebrospinal fluid. Bioanalysis. 2024;16(21-22):1155-1166.
11. Metzger M, Conrad S, Skutella T, Just L. RGMa inhibits neurite outgrowth of neuronal progenitors from murine enteric nervous system via the neogenin receptor in vitro. J Neurochem. 2007;103(6):2665-2678.
12. Zappulli V, Friis KP, Fitzpatrick Z, Maguire CA, Breakefield XO. Extracellular vesicles and intercellular communication within the nervous system. J Clin Invest. 2016;126(4):1198-1207.
13. Kim S, Teramachi J, Hiasa M, et al. Myeloma cell growth suppression by osteoblast-derived extracellular vesicles: the creation of a non-permissive niche for myeloma cells by bone-forming osteoblasts. Haematologica. 2025;110(6):1395-1401.
14. Zhang M, Xian HC, Dai L, Tang YL, Liang XH. MicroRNAs: emerging driver of cancer perineural invasion. Cell Biosci. 2021;11(1):117.
15. Hu B, Lv X, Chen H, et al. Sensory nerves regulate mesenchymal stromal cell lineage commitment by tuning sympathetic tones. J Clin Invest. 2020;130(7):3483-3498.

Figure legends

Figure 1. SN neurite-outgrowth promoting activity by MM cells.

(A) SN distribution in bone marrow. The indicated MM cell lines ($1x10^4$ cells) were inoculated into the bone marrow cavity of the tibiae of the right hind legs in SCID mice (CLEA Japan, Tokyo, Japan) (n=5 per group). Tumor-bearing tibiae (right) and intact contralateral tibiae (left, control) were resected 4 weeks after the inoculation. The samples were fixed and demineralized, and subjected delipidation in CUBIC-L for 3 days, followed by treatment with 0.1% collagenase A for 15 minutes. Subsequently, the samples were incubated for 2 weeks in an antibody reaction buffer with anti-CGRP antibody diluted 1:1000. They were post-fixed in 1% PFA at 4°C for 1 day, and then embedded in 1% agarose gel. The embedded samples were cleared using CUBIC-R for 2 days and imaged using a light-sheet fluorescence microscope (MuVi SPIM LS&CS, Bruker Luxendo GmbH, Germany) to visualize CGRP-positive sensory nerves. Three-dimensional reconstruction of the acquired images was performed using Imaris software (version 10.2.0, Oxford Instruments KK, Tokyo, Japan). (B) Primary dorsal root ganglion (DRG) cells were isolated from C57BL/6J mice, and enzymatically dissociated in 2 mg/mL collagenase type III at 37 °C for 120 minutes, followed by 0.05% trypsin-EDTA at 37 °C for 10 minutes to obtain a single-primary DRG cell suspension. The indicated MM cell lines were cultures for 2 days at $5x10^5$/mL, and culture supernatants were harvested. The culture supernatants were added at 20% to the neural cell line Neuro2a in the presence of NGF at 10 ng/mL and primary DRG cells. After culturing for 2 days, photos of the cells were taken after staining with calceinAM, and the length of the longest neurite from each cell was measured using NeuronJ (NIH, Bethesda, MD, USA). The representative photos of Neuro2a cells were shown (left panels). Original magnitude, x100. Size bars indicate 100 μm. (C) Recombinant NEO1 was added at 100 ng/mL to the neural cell line Neuro2a in the presence of NGF at 10 ng/mL and primary DRG cells, and after culturing for 3 days, the length of the longest neurite from each cell was measured using NeuronJ. Representative images of Neuro2a cells (original magnitude, ×100) and DRG neurons (×40) are shown. Size bars indicate 100 μm. (D) To deplete soluble NEO1, conditioned media from the indicated MM cell lines were incubated for overnight at 4°C with constant mixing with either 20 μg/mL rabbit anti-human NEO1 antibody or normal rabbit IgG. After the incubation, protein G-agarose beads were then added and further incubated for 1 hour, followed by centrifugation at 12,000 rpm for 5 minutes at 4°C. The MM cell conditioned media with or without the immunodepletion of NEO1 were added at 20% to Neuro2a in the presence of NGF at 10 ng/mL. After culturing for 2 days, the length of the longest neurites from each cell were measured using NeuronJ.

(E) We created *NEO1*-knock-out (KO) RPMI8226 cell line in which the NEO1 gene was knocked out with CRISPR-based gene editing. A single-guide RNA (sgRNA) targeting human NEO1 (5′-TGACACCATCAGGATTACGT-3′) was delivered into Cas9-expressing RPMI 8226 cells via lentiviral transduction. After 48 hours of puromycin selection, single-cell–derived clones were established by limiting dilution. Loss of NEO1 protein expression was confirmed by immunoblotting (left). The KO and control cells were cultured for 2 days at $5x10^5$ /mL, and culture supernatants were harvested. The culture supernatants were added at 20% to the neural cell line Neuro2a in the presence of NGF at 10 ng/mL. rNEO1 at 100 ng/mL was added as indicated. After culturing for 2 days, the length of the longest neurite from each cell was measured using NeuronJ. Data are expressed as mean ± SD. $^*P<0.05$.

Figure 2. Soluble NEO1 induces SN neurite outgrowth through inhibiting RGM-a

(A) rRGM-a was added at the indicated concentrations to Neuro2a in the presence of NGF at 10 ng/mL. After culturing for 2 days, the length of the longest neurite from each cell was measured using NeuronJ. (B) rNEO1 or rRGM-a alone at 100 ng/mL, or both in combination were added to Neuro2a in the presence of NGF at 10 ng/mL and primary DRG cells. After culturing for 2 days, the length of the longest neurites from each cell were measured using NeuronJ. Data are expressed as mean ± SD. $^*P<0.05$. (C) Neuro2a cells were first differentiated into SNs with extension of their neurites in the presence of NGF at 10 ng/mL. Then, rNEO1 or rRGM-a alone at 100 ng/mL, or both in combination were added as indicated, and neurite retraction was analyzed over time under a phase contrast microscope. The photos were taken at the baseline and after treating for 30 minutes. Arrows indicate retracted neurites. (D) Actin polymerization (F-actin) was detected with phalloidin for the cells treated above in (C). The number of phalloidin-positive cells were counted under a fluorescein microscope. Data are expressed as mean ± SD. $^*P<0.05$.

Figure 3. SNs enhance MM cell growth.

GFP-expressing MM cell lines were generated by lentiviral transduction with the pLL-CMV-rFLuc-T2A-GFP-mPGK-Puro vector (System Biosciences, Palo Alto, CA, USA). The indicated GFP-expressing MM cell lines were cultured in triplicate at 5 $x10^4$/mL alone or cocultured with SNs derived from the Neuro2a or primary DRG cells in 24-well culture plates. The numbers of GFP^+MM cells were counted over time under a fluorescence microscope (KEYENCE BZ-X800). EVs were isolated from culture supernatants of Neuro2a-derived SNs and primary DRG cells. EV purification was performed using a material processed with an exosome-affinity component based on sodium polyacrylate, a

superabsorbent polymer (SAP) (EXORPTION®, Sanyo Chemical, Kyoto, Japan). After incubation, the SAP was filled into a filter column, then washed three times with PBS, and PBS was removed at 1000 rpm for 1 minute. The washed SAP was immersed in the extraction solution for 30 minutes to detach EVs from the SAP surface, and EVs were collected at 1,000 rpm for 1 min. EVs isolated from respective culture supernatants (10 mL) were resuspended in 1 mL (10× concentration). The indicated MM cell lines were cultured at 5.0×10^4 cells/mL in triplicate in culture media with or without the EVs. The EV solutions were added to the indicated wells to be diluted 1/10 (approximately 10^9 EV particles/mL). Viable cell numbers were counted at day 3. Percent changes from the baseline were compared.
(C) DRG cells were cultured for 2 days in the presence or absence of the miR-21 inhibitor miR-21-IN-3 (MedChemExpress, NJ, USA) at 10 μM. The cells were washed and cultured in the absence of miR21-IN-3 for another 2 days to collect culture supernatants for EV isolation. The indicated MM cell lines were cultured at 5×10^4/mL alone or with EVs isolated from the DRG cells pretreated with or without miR-21-IN-3. Values represent the mean ± SD. *P<0.05. (D) Pharmacological sensory denervation was performed in 4 week-old SCID mice by administering capsaicin (CPS) at a dose of 20 mg/kg body weight or a vehicle (PBS) for 5 consecutive days. Tibiae were resected and subjected to optical clearing with the CUBIC method. CGRP-positive SNs were visualized by a light sheet microscope (upper). After the CPS or vehicle treatment, the MM cell lines 5TGM1 and JJN3 transfected with Luc (luciferase) were inoculated into the right tibiae of SCID mice with or without the pharmacological sensory denervation. IVIS images were taken 4 weeks after the inoculation.
(E) *NEO1*-KO or control RPMI8226-Luc cells were inoculated into the right tibiae of SCID mice. 4 weeks later, right and left tibiae were resected, and subjected to optical clearing with the CUBIC method. CGRP-positive SNs were visualized by a light sheet microscope (upper). IVIS images were taken at 2 weeks after the inoculation (lower). Tumor areas with luminescence were measured. Px: pixels. Data are expressed as mean ± SD. $^*P<0.05$

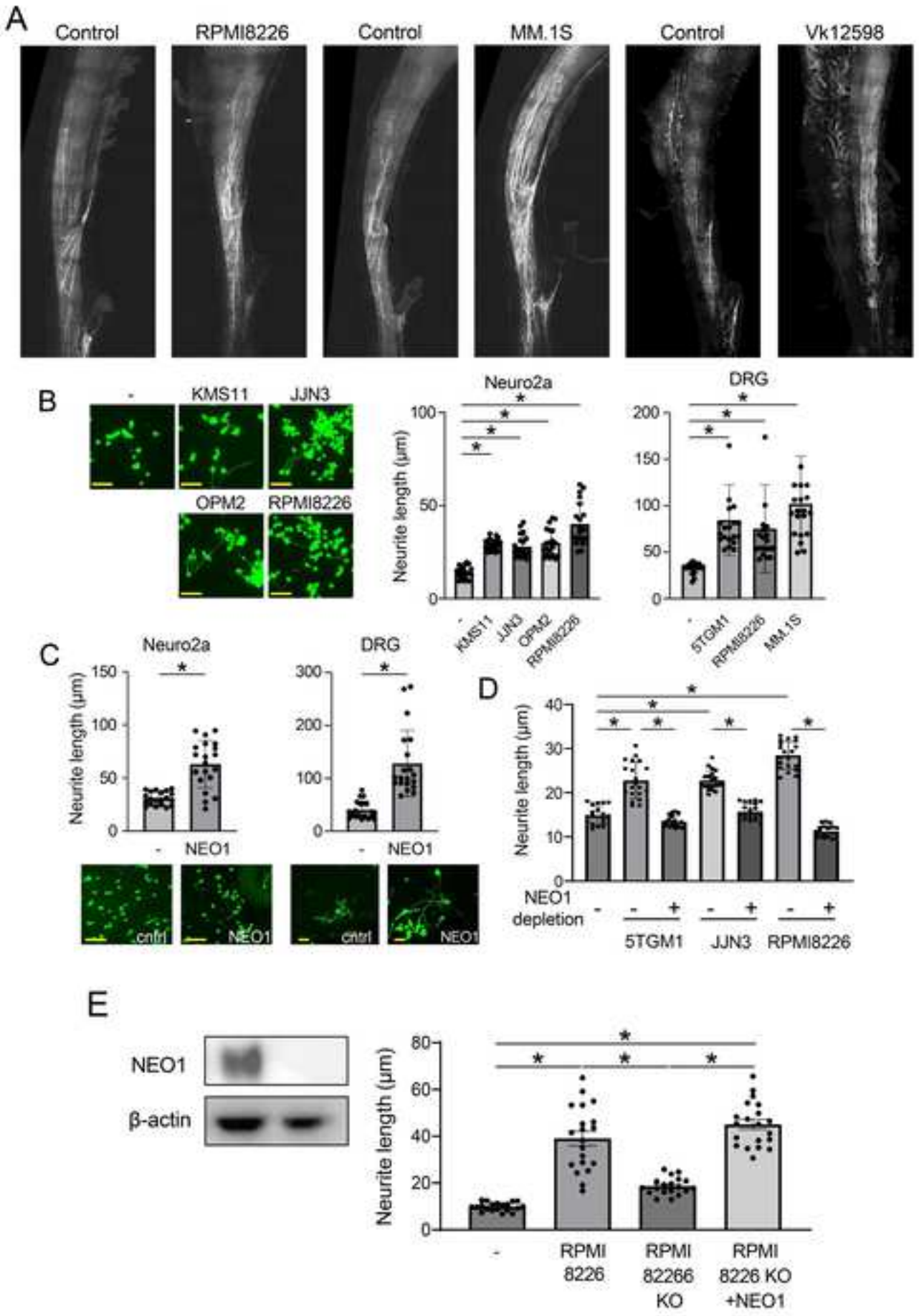
Figure 1
A
Control
RPMI8226
Control
MM.1S
Control
Vk12598
B
-
KMS11
JJN3
OPM2
RPMI8226
Neuro2a
DRG
Neurite length (μm)
-
KMS11
JJN3
OPM2
RPMI8226
5TGM1
RPMI8226
MM.1S
C
Neuro2a
DRG
Neurite length (μm)
-
NEO1
cntrl
NEO1
D
Neurite length (μm)
NEO1 depletion
5TGM1
JJN3
RPMI8226
E
NEO1
β-actin
Neurite length (μm)
-
RPMI 8226
RPMI 82266 KO
RPMI 8226 KO +NEO1

Figure 2

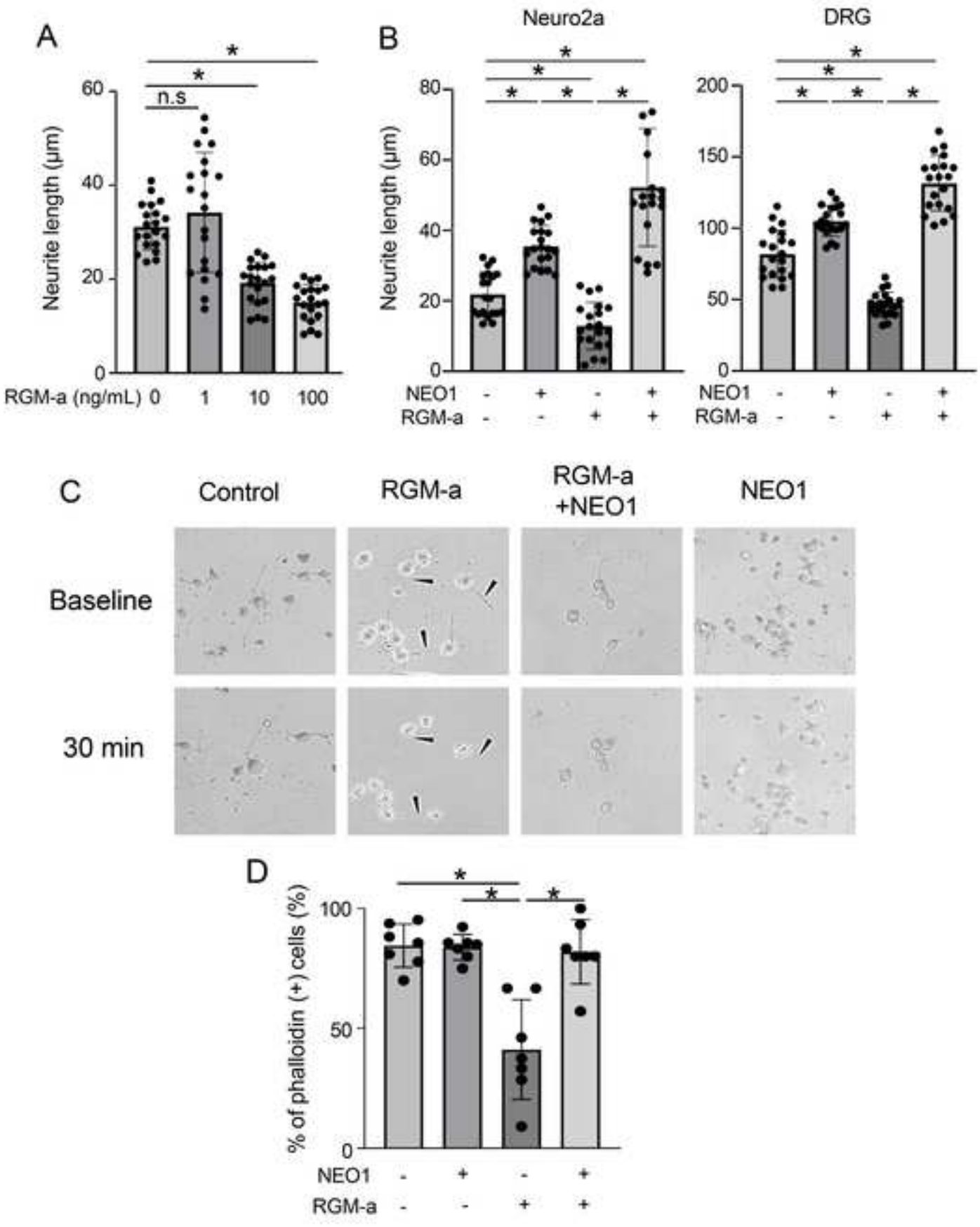
A
B
Neuro2a
DRG
C
Control
RGM-a
RGM-a +NEO1
NEO1
Baseline
30 min
D
Neurite length (μm)
RGM-a (ng/mL) 0 1 10 100
n.s
NEO1
RGM-a
% of phalloidin (+) cells (%)

Figure 3

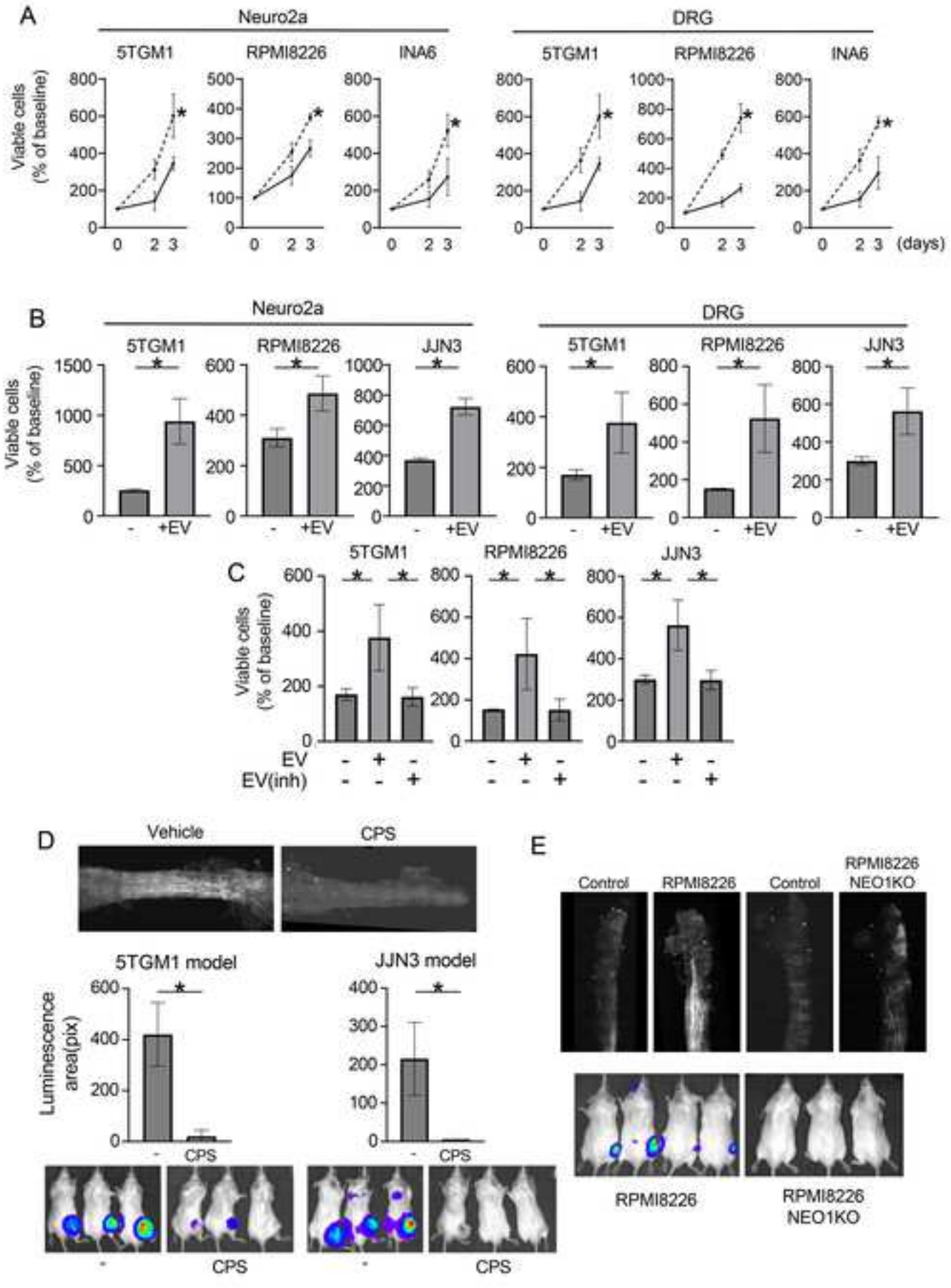

Supplementary Figure 1

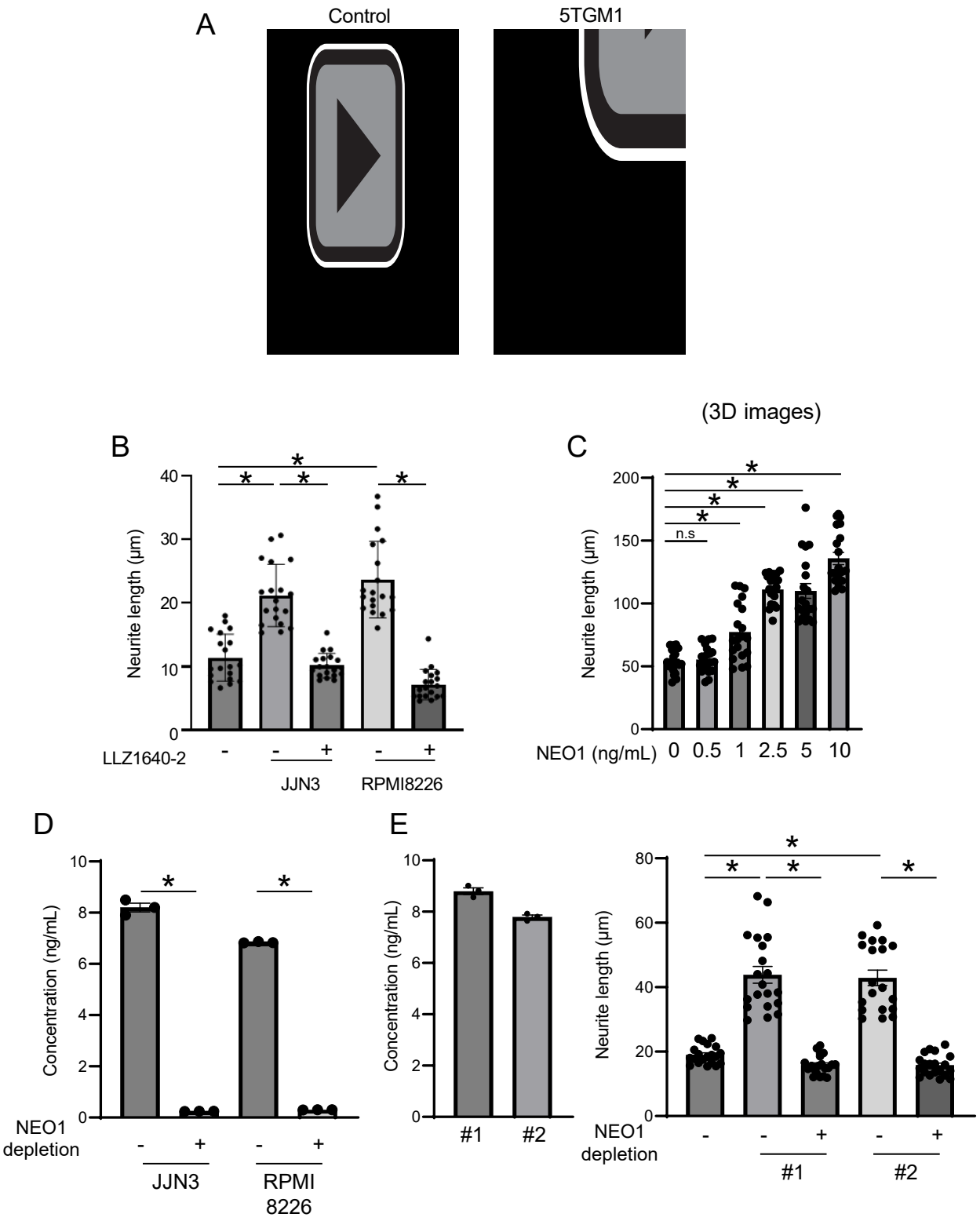

Supplementary Figure 1.

(A) 5TGM1 MM cells were inoculated into tibiae in right hind legs of SCID mice. Tumor bearing tibia (right) and intact one (left) as a control were resected from the same mice at 4 weeks after the inoculation, and subjected to optical clearing with the CUBIC method. CGRP-positive SNs were visualized by a light sheet microscope. Images were displayed in three dimensions. (B) JJN3 and RPMI8226 MM cells were treated for 24 hours in the presence or absence of the TAK1 inhibitor LLZ1640-2 at 5 μM. After washing to remove LLZ1640-2, viable cell numbers were counted, and the viable cells were cultured at $5x10^5$/mL. After culturing for 2 days, their culture supernatants were harvested. The culture supernatants were added at 20% to the neural cell line Neuro2a in the presence of NGF at 10 ng/mL. The length of the longest neurite from each cell were measured using NeuronJ. Data are expressed as mean ± SD. *P<0.05. (C) Recombinant NEO1 was added at the indicated concentrations to the neural cell line Neuro2a in the presence of NGF at 10 ng/mL. After culturing for 7 days, the length of the longest neurite from each cell was measured using NeuronJ. (D) Concentrations of

NEO1 in pre- and post-depletion supernatants were measured by ELISA. (E) Concentrations of NEO1 in culture supernatants of primary $CD138^{+}$MM cells from patients with MM were measured by ELISA (left). The conditioned media with or without the immunodepletion of NEO1 were added at 20% to Neuro2a in the presence of NGF at 10 ng/mL (right). After culturing for 2 days, the length of the longest neurites from each cell were measured using NeuronJ.

Supplementary Figure 2

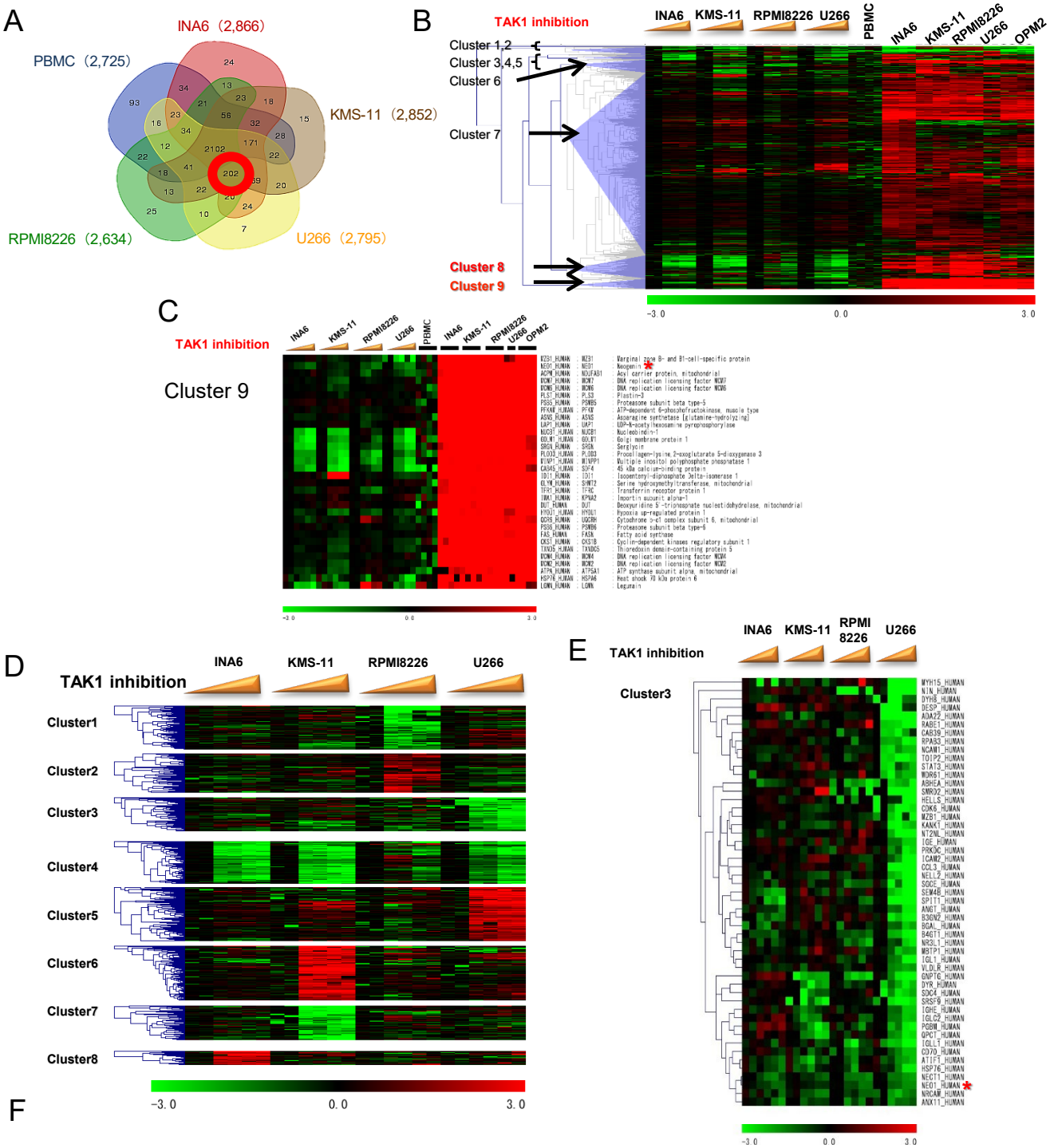

Protein name	Relative abundance (ratios of MS intensity vs PBMC (log2))					Change by TAK1 inhibition (MS intensity ratio (log2))			
	PBMC	INA6	KMS11	RPMI8226	U226B1	INA6	KMS11	RPMI8226	U226B1
Neogenin1	-0.066	4.644	4.674	5.145	6.887	-1.227	-0.560	-1.390	-1.692
Cyclin-dependent kinases regulatory subunit 1	-0.311	3.174	5.062	4.717	4.489	-0.188	-0.726	-0.255	-0.549
Neuroserpin1	-0.146	3.978	1.646	3.955	2.378	-3.542	-4.002	-0.007	-3.020
ADAM9	-0.051	1.507	1.664	3.801	1.942	-3.053	-3.100	-2.663	-3.728
V-type proton ATPase subunit S1	-0.024	2.234	2.332	4.633	2.749	-3.606	-3.560	-2.025	-3.317
Alpha-galactosidase A	-0.042	1.623	2.072	5.163	1.737	-1.824	-3.963	-1.393	-0.634
Glucosylceramidase	-0.046	1.997	2.498	4.936	1.027	-3.261	-3.989	-2.108	-3.911
Palmitoyl-protein thioesterase 1	-0.107	4.189	3.890	5.499	3.618	-2.121	-2.246	-1.164	-1.906
Hydroxymethylglutaryl-CoA synthase	-0.117	3.588	3.976	6.311	4.185	-3.915	-0.157	-0.307	-1.003
Stromal cell-derived factor 2	-0.045	0.313	2.728	2.528	2.595	0.392	-0.253	-3.844	-1.092
Beta-galactosidase	-0.092	0.871	0.574	2.550	2.204	-0.050	0.503	-0.314	-2.244

Supplementary Figure 2.
MM cell-specific, TAK1-dependent proteins were selected by a comprehensive secretome analysis for culture supernatants. The indicated MM cell lines and peripheral blood mononuclear cells (PBMC) were cultured in serum-free medium ($5x10^5$ cells/mL) in the presence or absence of the TAK1 inhibitor LLZ1640-2 at 0.625-10 μM for 24 hours. Their conditioned media were then centrifuged (15,000 rpm, 15 minutes, 4°C) and filtered using a 0.2 μm membrane filter. The secreted proteins were cleaned up by chloroform/methanol, suspended in 10 mM Hepes buffer (pH 8.9) containing 6M urea/2M thiourea and digested with Lys-C protease. The samples were further digested with trypsin as described previously. Each 1 mg digested protein was subjected to mass spectrometry (MS) using an Orbitrap Fusion Tribrid Mass Spectrometer (Thermo Fisher Scientific) in a data-dependent acquisition mode as described previously. The MS data obtained were processed with MaxQuant software (ver. 1.5.3.30), and Andromeda search engine was used to search the UniProt KB FASTA database (20,195 reviewed entries, Ver. from April 2017). (A) VennDiagram of proteins secreted from MM cell lines and PBMC. The numbers of proteins detected are shown in parentheses. Proteins detected in all 4 MM cell lines but not in that of PBMC were circled (202 proteins). (B) Cluster analysis of proteins secreted from 4 MM cell lines and the effects of the TAK1 inhibitor LLZ1640-2 on the secretome. Only proteins showing significant increase (LFQ ≧2 reported from MaxQuant software) in the secretome of 4 MM cell lines compared to that of PBMC were selected in the analysis (750 proteins, right panel). The effect of the TAK1 inhibition on secretion levels of those proteins were analyzed in the secretome of four MM cell lines (left panel). Data from 4 independent measurements were used for the clustering individually, and signals that were originally zero were imputed with random numbers from a normal distribution. Heat map analysis and hierarchical clustering (Manhattan distance) were performed using MultiExperiment Viewer (MeV software version 4.9, https://mev.tm4.org/#/welcome). (C) Cluster 9 contains proteins with high basal secretion levels in all of the 4 MM cell lines showing a decrease upon the LLZ1640-2 addition. Neogenin1 was detected in the cluster 9, and marked with an asterisk. (D) We also performed K-means clustering analysis of proteins secreted from four MM cell lines showing significant effects of TAK1 inhibition on the secretome. Secreted proteins from four MM cell lines were cultured with varying concentrations of LLZ1640-2. Total 2,872 proteins were identified with ≧2 RazorUnique peptides reported from MaxQuant. Of these 2,411 proteins were quantified with LFQ ≧2 reported from MaxQuant software). Signals that were originally zero were imputed with random numbers from a normal distribution. After imputation, the quantitation values were evaluated with one-way ANOVA, and total 1,533 proteins with significance ($p<0.05$) were selected for clustering. (E) K-means clustering analysis of proteins secreted from four MM cell lines showing significant effects of the TAK1 inhibition on the secretome. The proteomics data files are available on request from the corresponding authors. (F) The selected proteins are listed according to high basal secretion and TAK1 dependency. Average ratios of abundance of basal secretion and fold change from their baselines with TAK1 inhibition (10 μM) are tabulated in each MM cell line.

Supplementary Figure 3

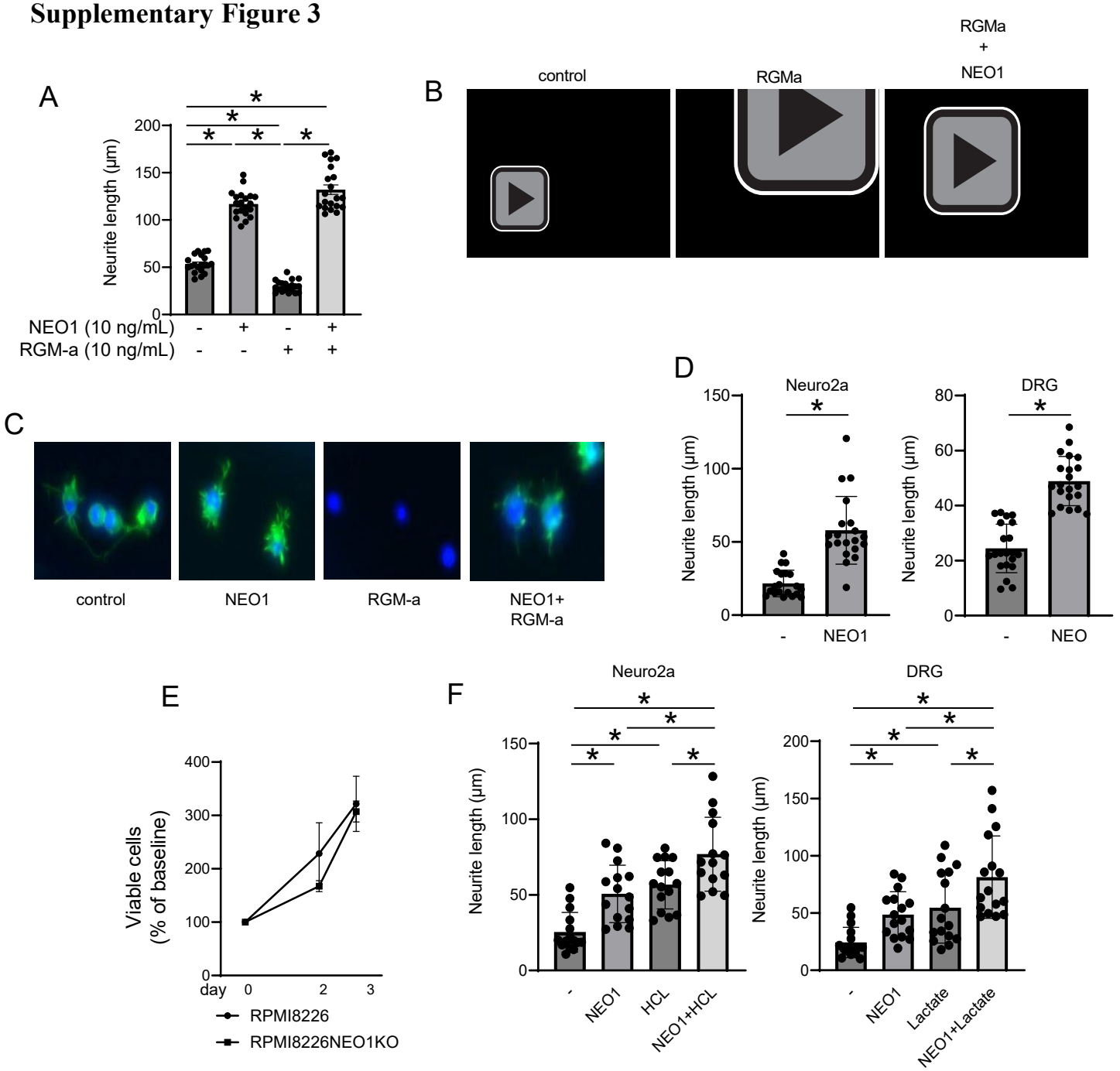

Supplementary Figure 3.
(A) rRGM-a was added at 10 ng/mL to Neuro2a in the presence of NGF at 10 ng/mL. After culturing for 2 days, the length of the longest neurite from each cell was measured using NeuronJ. (B) Neuro2a cells were differentiated into SNs with neurite extension in the presence of NGF at 10 ng/mL. The cells were stained with calcein AM. Recombinant NEO1 (NEO1) or recombinant RGMa (RGMa) at 100 ng/mL alone, or both in combination were added, and neurite contraction was observed over time under a phase-contrast microscope. Time-lapse images were recorded for 2 hours. (C) Actin polymerization (F-actin) was visualized using phalloidin (green). Nuclei were counterstained with DAPI (blue). Representative images are shown. (D) Recombinant NEO1 (100 ng/mL) was added to Neuro2a in the presence of NGF at 10 ng/mL and primary DRG cells under a serum-free condition. After 3 days, the longest neurite of each cell was measured using NeuronJ. (E) *NEO1*-KO and control RPMI8226 cells were cultured at 5×10^4/mL. Variable cell numbers were counted. (F) Neuro2a cells were cultured in 24-well plates for 2 days in the presence of NGF at 10 ng/mL under acidic conditions (pH 6.8) prepared by lactic acid (Sigma-Aldrich) or HCl. Recombinant NEO1 was added at 100 ng/mL as indicated. After 2 days, the longest neurite of each cell was measured using NeuronJ. Data are expressed as mean ± SD. *P<0.05.